MICROSTRUCTURE AND MORPHOLOGY OF Cu Ag/PbO NANOPARTICLES SYNTHESIZED BY PULSED LASER PLAL

Mohamed. A. Karem[1] and Raghad. S. Al-Khafaji[2*]

[1]Master Student ,[2]Department of Physics, College of Education for Pure Sciences/ bn- Al-Haithem University of Baghdad, Baghdad,Iraq.

[1]**mhma15692@gmail.com,** [2,*]correspondence; E-mail: raghadsubhiabbas@yahoo.com

ABSTRACT: *PbO-doped Cu and Ag (noble metals) crystalline colloidal nanoparticles were synthesized by pulsed laser ablation (PLAL) of PbO: Cu-Ag ceramic pellet targets in (DIW) deionized water. The experiment was achieved systematically by using a pulsed Nd-YAG laser of wavelength (λ= 1064 nm) and pulse duration of 6ns, 300 number of pulses for 400 mg of output energy. The structural properties of prepared films were characterized as a function of Cu-Ag content (15-85 wt. %) in the target.*

Calculated lattice constraints 'a' and 'c' are found decreased with increase in Cu concentration while these parameter increase in Ag-doping in $PbO_{1-x}Ag_x$. Rietveld method is a good performance for concluding structural data details from diffraction powder, we get (Goodness-of-fit) (1.1, 1.2) for PbOCu and PbOAg respectively were considered a fine analysis. An SEM and TEM imaging were examined for the morphology of prepared nanostructure and to determine crystallite size and particle distribution, which TEM revealed nanoparticles of PbOCu 12.6339*nm and for sample PbOAg (85%)* 9.1624*nm.*

Keywords: nanoparticles, colloidal, Rietveld method, TEM**,** Microstructure and morphology properties.

1. INTRODUCTION

In the past, nano-structures like nano-crystals, nano-wires, and nanobelts have been manufactured by several ways including solvothermal, evaporation of thermal, sole gel process, sputtering, deposition chemical vapor (CVD) and lately, by one-pot methodology [1-3]. Nevertheless, the production of numerous nanoparticles (NPs) utilizing (PLAL) Pulse Laser Ablated in Liquid, is an alternative to those chemical process, and it is distinguished by its relative easiness to produce pure nanoparticles, NPs, with colloids missing impurities. PLAL has been employed to generate, excite, fragment and conjugate elemental, nano-alloy, ceramic or semiconductor NPs. The laser ablation in liquid medium for the solid target comprises several processing of NPs establishment. A plasma plume is created with the interaction of the beam of laser high energy onto the target surface. The nanoparticles NPs are then ejected immediately from the target when laser pulses of short and ultra-short are used. Afterward, nucleation and condensation procedures occur in the growing plasma plume and nanoparticles are thus grown in the liquid. In particular, PLAL is considered to be very simple, efficient, fast, and environmentally-friendly technique for suitably synthesizing colloidal solutions nanoparticles for a wide range of materials and a wide range of nanoparticle kinds. Also, ablation by pulsed laser was utilized to induce re-shaping of irregular particles shaping to spherical particles by melting condensation and chemical reduction.

Noble metals nanoparticles demand a lot of attention from researchers. Nanoparticles of gold (Au) silver (Ag) and copper (Cu), for example, have various applications in the fields of material science, optics, chemistry, biology, and medicine. A large number of researchers report synthesizing by PLAL, such as Ag, Au, and Cu nanoparticles [4-8].

The principal goal for this research is to explore the production of colloidal (Cu-Ag)-doped PbO nanoparticles using PLAL technique in Deionized (DI) water medium. We have mainly focused on the Cu/PbO and Ag/PbO targets of various concentrations to investigate the synthesis of (Cu -Ag) -doped PbO nanoparticles, and subsequently study microstructure and morphology properties.

2. EXPERIMENTAL SETUP

Commercial micro powders from lead oxide (Alherich Sigma Company), copper and silver (BDH Chemicals Ltd England). We have used a mixture of PbO:Cu and PbO:Ag with various concentrations of doped noble metal (x=15,20,30,50,75,85 wt%), then pressed (4-6 Ton) pellet target (diameter 1.5 cm and thickness with 0.3cm), to synthesize nanoparticles colloids by employed laser ablation in deionized (DI) water. The target was down occupied in 25 ml beaker keeping the water level consistently higher above the surface of the target at 1 cm for the duration of ablation laser with the intention to keeping the efficiency of laser ablation constant. The pressed targets were vertically irradiated by (Q-switched Nd-YAG laser DIAMOND-288 pattern EPLS), operating at the wavelength (λ) = 1064 nm, pulse duration of 6ns, 300 number of pulses for 400 mJ of output energy. The laser beam was then focused on the targets using a lens with a focal length of 20 cm. The target and glass container was rotated during the process, to avoid a deep crust due to repeated laser pulses on the same spot.

Films of the nanoparticles colloidal solutions were prepared for XRD, X-ray diffraction technique for structural examinations and morphology by drop coating of individual solution onto a glass substrate. Dropping was repeated several times until a clear film was formed, with consideration of sonicating the suspension solutions for 5 min before the deposition. The XRD tests were carried out on a diffractometer provide with a Cu –Kα X-ray tube (Shimadzu XRD – 6000), in the angular range 2θ = 10–80. As well as, the morphology and calculated size distribution of the produced nanoparticles were examined using an (SEM, FEI Company Inspect S50-Model), scanning electron microscope equipped with an energy-dispersive X-ray spectrometer (EDS, Burker Company-Germany X Flash 6l10-Model)). Drops of the colloidal solutions of nanoparticles (with consideration of sonicating the suspension solutions for 5 min before the deposition) were prepared and dried separately on model grid of copper-gold coated (contains about 200 meshes) to describe their morphology, structure and size using transmission electron microscopy(TEM of Model CM10 PW 6020, Philips-Germany).

3. RESULTS AND DISCUSSIONS

During preparation of the sample in PLAL progression, the target surface immersed in the liquid was subjected to the laser pulse, a spark plume created and accompanied by the creation of a plasma plume, visible to the examiner nearby the target surface. The spark of plasma formation emitted light and cracking noise, the solution appeared colorless and it began to change to yellow within a few minutes, indicates that Nano sized colloidal particles with high concentration have been produced. X-ray diffraction patterns were used for investigating the phase compositions of the prepared samples, that one could observe the deposition prepared films demonstrated as the polycrystalline tetragonal structure of PbO_2 (ASTM data card 00-041-1492). Important changes, detected in the X-ray diffraction spectrum, noticeable themselves by increasing of peak intensity in crystal plane and decreasing in the peak intensity consistent to other planes. XRD in fig.1 illustrates $PbO_{1-x}Ag_x$ compound. The peak positions of the planes attributed to PbO_2 phases were shifted to lower 2θ values with increasing the amounts of Cu content. For PbO pure nanoparticles diffraction peaks were located at angle 2θ= 34.2569° and 23.6737°, Cu 20% peaks of diffraction were situated at 2θ= 34.1587°, Cu 50% addition the diffraction peaks positioned at 2θ=34.3785° and 22.5861°, with Cu 75% peaks of diffraction were located 2θ=34.0688° and 23.7535°, and for Cu85% diffraction peaks were located at 2θ= 34.1487° and 21.9077°. There are phases result to formation of compound Pb (Cu_2O_2) nanoparticles (card number 96-153-5316**) at** 2θ=16.71°, 27.40°, 33.67° and 43.93° reflected planes 111,220,222 and 420 respectively. It is noticed from fig.1 the broadening (full width at half maximum) the increase with increasing copper addition. For pure (PbO) at 2θ= 23.6737° FWHM 0.32000, Cu 75% at 2θ=23.7535° FWHM 0.66000, Cu 50% addition at 2θ=22.5861° FWHM 1.50000. Furthermore, PbO pure nanoparticles at 2θ=34.2569° FWHM 0.77670, Cu 20% 2θ= 34.1587° FWHM 1.32000 and Cu 50% 2θ=34.3785° FWHM 1.04000. This broadening of FWHM is attributed mainly to the large lattice mismatch between the lead oxide and added copper metal. Fig.2 represents the XRD pattern $PbO_{1-x}Cu_x$ phase.

The peaks positions of 2θ=29.06°, 34.19° and 48.19° attributed to phase Ag_2PbO_2 relative to planes 121,130 and 12-3 respectively. Peak positions of the planes attributed to PbO_2 phases shifted to lower 2θ values with increasing the amounts of Ag content. For Ag 15% diffraction peak was located at 2θ=34.18°, Ag 20% 2θ=34.13°and Ag 50% 2θ=34.14°. On the other hand, fig.2 revealed the broaden decrease with increasing silver metal addition. At 2θ=34.18° Ag15% FWHM 0.41and at 2θ=34.14° Ag 2% FWHM 0.37.

The Ag ions (1.28A° diameter) were substituted into the Pb^+ (1.23A°) in the lattice of PbO_2 film. The broadening of Bragg peak is combined of both instrument and tasted sample dependent effects, i.e., crystal faultiness, and distortion for strain-induced peak broadening. It be illustrated from XRD analysis of prepared $PbO_{1-x}Ag_x$ film there is increase in the peaks intensity (I) at a mainly strongest angle 2θ~34A° with decrease in Ag concentration (I reached maximum for Ag50% and Ag30%) due to formation scattering factor is depending on atomic number (Z) (atomic number of lead higher than that of silver) also, may be assign to diffraction peaks angles PbO_2 nanoparticles phase identified with phase Ag_2PbO_2 compound nanoparticles in prepared film.

There are two methods of indexing structure mathematical and analytical. In this work, the produced predominating structure is tetragonal of PbO film with a various concentration of copper and silver. A relative is developed by scrutinizing plane-spacing equation and equation of Bragg's law, which decides the Miller indices of some particular crystal system, for a tetragonal system, this manifestation can be inscribed as [7]:

$$\sin^2\theta = \left(\frac{\lambda^2}{4}\right)\left(\frac{h^2+k^2}{a^2}+\frac{l^2}{c^2}\right) \quad \text{.....1}$$

Using Match software which depending least square it can be calculated lattice constants 'a' and '*c*' for all the samples which are listed in table 1 .It can explain this parameter are decreased with increase in Cu concentration in $PbO_{1-x}Cu_x$ film , These variations may be owing to smaller of ionic radius for Cu2+ (0.57A°) than that of Pb^{2+} (1.23A°) [9]. Volumes of the unit cell for all the samples are also listed in table 1. ascribable by decreasing tendency of lattice constant parameters '*a*' and '*c*', the volume for the unit cell are similarly decreased with increasing Cu contents, as stated previously [10-12]. Furthermore, the table was clarification lattice constants 'a' and '*c*' for all the prepared samples $PbO_{1-x}Ag_x$ are increased with increase in Ag concentration, which attributed to the larger ionic radius of Ag2+ than that of Pb2+. Subsequently, volumes of the Unit cell of all the samples are also increased with increasing Ag contents. The crystallite size (l) of the prepared grown films it can be calculated by using the Debye-Scherrer formulation [11]

$$\beta_{1/2}(2\theta) = \frac{K\lambda}{L\cos\theta} \quad \text{....2}$$

Where:

L is the average size of the crystallites;

λ = Wavelength of radiation. (Cu Kα = 1.5418 Å).

$\beta_{1/2}$ = Full width half maxima (FWHM, in radians).

θ = the peak position (in degrees). K (the Scherrer constant) is constant of proportionality, be contingent on the shape for the crystallization, and distribution size (round up to 1).

Table 1 has been the obvious behavior of crystallite size; it can be deduced for synthesized $PbO1_{-x}Cu_x$ film the crystallite size decreases with increasing Cu doping with enhanced crystallinity. A similar trend was previously observed [8].It was basically due to the replacement of the Cu ions were substituted into the Pb^+ in the lattice of PbO_2 film. Moreover, crystallite size increase with increasing Ag-doping in $PbO_{1-x}Ag_x$ film, refer to substituted Ag ions larger than that ions Pb^+ in the lattice of PbO film. The Rietveld manner is a well-recognized technique for deducing structural details from diffraction powder information [11]. This method was established on a least-squares fit among step-scan data of an examined diffraction pattern and a simulated X-ray-diffraction (XRD) pattern. In this study, the crystalline structure of the PbO/Cu-Ag

Tetragonal was scrutinized in detail by the refinement Rietveld profile process in the reflex module (Fig. 3and 4). Patterns of XRD for these synthesized samples have refined employing the space group -p 4n 2n. The refinements of the Rietveld method allowable the determination of the parameters of lattice and crystal structural. The profile parametric for the function of pseudo-Voight were utilized to define the shape of the diffraction peaks and the refinement of the structure was carried out by contemplating the PbO structural assumption. In the -p 4n 2n space group of tetragonal structure. Profile of peaks was defined with the function of (Thompson-Cox-Hasting) for our samples. Fig.3 and Fig.4 are given a relationship between the experimental and calculated patterns of XRD for the samples Cu6 and Ag6. The superiority of the agreement between calculated and observed profiles was measured by adjusting of conventional factors. Two sets of the index were calculated, conferring to the meaning of N integer. The first set N was the whole number for points which used in the process of refinement. In the second set merely individuals points where are Bragg donations are taken into account.

Definition of the index is as following:

R- Pattern (profile)

$$R_p = \Sigma |y_i(obs) - y_i(calc)| / \Sigma |y_i(obs)| \quad \ldots 3$$

R expected

$$R_E = [(N-P)/\Sigma w_i \{y_i(obs)\}^2]^{1/2} \quad \ldots. \; 4$$

Where, N and P are the number of profile points and refined parameters, respectively

$$R_{wp} = [\Sigma w_i \{y_i(obs) - y_i(calc)\}^2 / w_i \{y_i(obs)\}^2]^{1/2} \quad \ldots 5$$

Goodness-of-fit

$$\chi^2 = (R_{wp}/R)^2 \quad \ldots\ldots 6$$

X ^{2}lesser than 2 was reflected a fine analysis, so we have made a very good analysis for synthesis samples. The several R factors RELIABILITY FACTORS are tabulated in Table 2. The values for R factor like Rp are found to be high. Similarly, high values of factors (R) for materials of nanocrystalline have been detected with the other authors [11-12]. It might be due to the high noise-to-signal percentage of XRD diffraction for nanocrystalline materials. Nevertheless, a low value of (goodness of fit) χ^2 which condemn the goodness of analysis refinement is noticed. Diffraction data pattern for nanocrystalline materials, diffuse scattering is governing

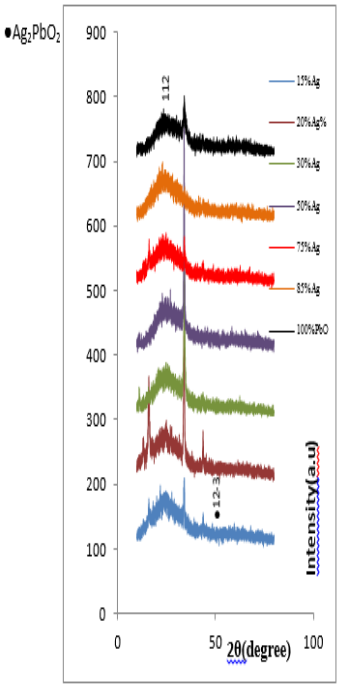

Fig. 1 XRD pattern for prepared PbO/Ag film

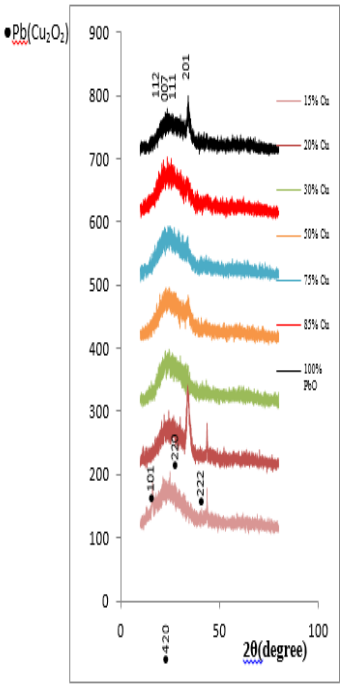

Fig. 2 XRD pattern for prepared PbO/Cu film

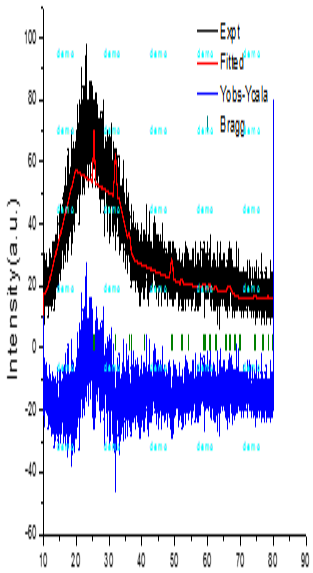

Fig.3 Rietveld method XRD 85%Ag

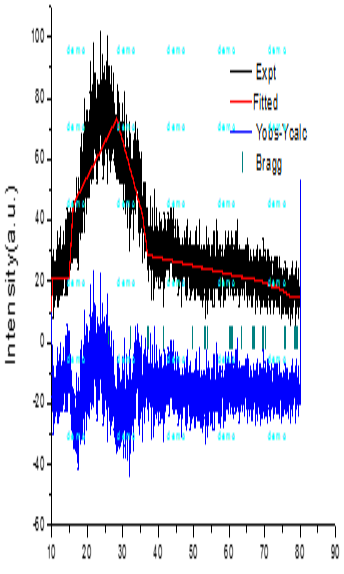

Fig.4 Rietveld method XRD 85%Cu

than in individuals for crystalline materials bulk, and it was owing to the large ratio of volume atoms to surface. Diffuse scattering comes to be substantial at the nanoscale whereas scattering of Bragg gets reduced which leads to weakening in crystallinity and high R factors.

Table1 Concentrations sample nanoparticles, lattice constants and crystallite size from XRD

sample	Con %	Lattice constants (Å□)		Volume (Å³)	crystallite size (nm)
		a	c		
PbO	100	3.48760	8.64300	105.128	27.73906
C1	15	4.02738	11.58780	187.952	13.06706
C2	20	3.83678	10.68920	157.350	11.30961
C3	30	3.81565	10.55741	153.707	10.70540
C4	50	3.79751	10.01121	144.372	7.30976
C5	75	3.78023	11.16160	159.500	14.86390
C6	85	3.76614	11.11720	157.684	12.88254
A1	15	5.83331	10.25011	348.785	20.21315
A2	20	5.89770	10.21730	355.387	16.51704
A3	30	6.09760	10.08570	374.993	19.69971
A4	50	6.11211	11.10310	414.787	57.87615
A5	75	5.86600	11.37310	391.348	12.04397
A6	85	5.72496	11.90121	390.063	20.16605

Table 2 Reliability factors form Rietveld method

Sample	Con %	R_p	R_{wp}	R_{exp}	GoF-index	Phase	Space group
Cu	85	15.1	20.0	17.6	1.1	Tetragonal	-p 4n 2n
Ag	85	16.1	20.4	17.5	1.2	Tetragonal	-p 4n 2n

Table 3 Crystallite size of nanoparticles prepared form SEM and TEM

Sample	crystallite size(nm)	crystallite size (nm)
PbO	40.7844	--
C1	39.9627	--
C6	36.4186	12.6339
A1	40.5421	--
A6	37.2877	9.1624

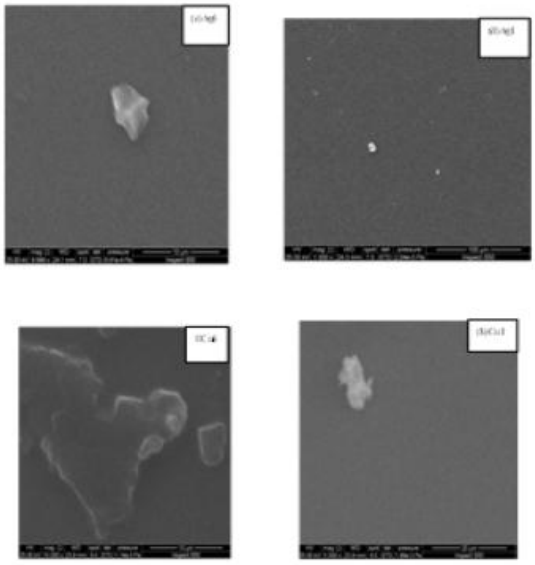

Fig.5 SEM images for prepared nanoparticles PbO/Cu and PbO/Ag

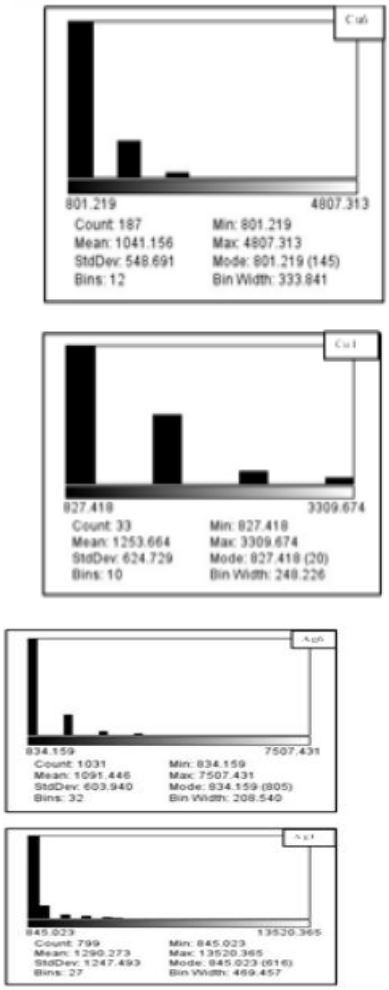

Fig.6 Statistical area distribution of synthesized nanoparticles from SEM

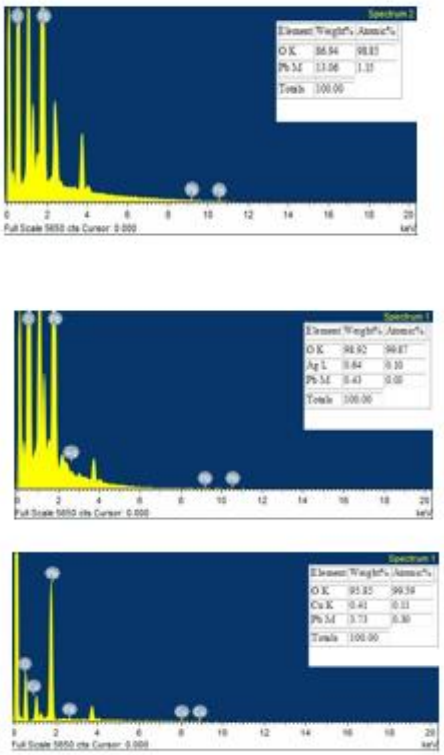

Fig.7 EDX spectrums for pure (a)PbO, (b)Pb/Ag and (c)PbO/Cu.

Imaging of SEM was employed to define and characterize the influence of the synthesis parameters like, laser pulses number, laser production energy, nature of liquid medium on the morphology of synthesized nanoparticles and to conclude its distribution of size. In Fig. 5 features images (SEM) are illustrated morphology of deposited samples made in (DI) water. It seems homogeneous, structures of mesh-like with nanoparticles preserved their spherical forms with spare concentration for nanoparticles of colloidal were gotten. PbO pure, $PbO_{1-x}Cu_x$ and $PbO_{1-x}Ag_x$ nanoparticle of various concentrations (15-85wt%), formation processes in (PLAL) are designated with dynamical development mechanisms comprising growth process of diffusion or amalgamation diffusion process[10]. Construction of sphere-like (Cu and Ag)-doped PbO nanoparticles may be credited to two processes describing the growth of nanoparticles [7]. First was that which it found that the ions from plasma plume of laser ablated may control the nanoparticles growth as particles of dopant. The second was that growth of nanoparticles upon PLAL is set through the energy of surface for the compose crystals with different of orientation which could result in the favored formation of nano sphere. Furthermore, temperature and pressure are inclines may too induce 2D anisotropic of growth directional in addition to, the high for nucleation of temperature.

Size and particle distribution were examined of the deposited films and quantified by visual basic software using several SEM images. Fig. 6 show the histogram figures of area distribution of PbO pure, $PbO_{1-x}Cu_x$ and $PbO_{1-x}Ag_x$ compound nanoparticle of various concentrations (15-85wt%), observed from these images that the average particles size Ag NPs is around 37-40 nm, and for 36-39nm Cu NPs. Nanoparticles which produced from gaseous phase what is the instance in nanoparticles synthesis procedures by PLAL. It put on at whatever time particle growth be subject on atoms which diffusion and drift to a growing for nanoparticles. Final dispersal is determined with the obtainable time of growing for nanoparticles. In our study during PLAL, the targets were stirring in order to evade drilling and probable effects of heating. Generally, the crater effects the size of the particle (volume resembles a number of employed laser pulses). Dependence belongs size of a particle on a number of used laser pulses could be ascribed for heating permanently of the target upon extended laser ablation as the laser pulse was breaking the similar spot during PLAL so the threshold of energy for ablation decreases supporting the ablation rate and thus ablated species density in the phase of gaseous. Less-likely picture as there is no indication to provision it. As of the dependency of volumes for craters and intensity of photo absorption on a number of functional laser pulses such deduction might not be built because of volumes and photo absorption will increase with the pulses number rather exponentially than linearly. The more-likely situation was that on laser ablation the craters will be larger and deeper so that ablated material is enclosed by its walls and do not have much area to disperse around. Once laser pulse strikes onto the target, a dynamic plasma plume containing the atoms, ions, and molecules are formed and it develops. Formation of particles can be designated with the mechanism of dynamic formation [5-11]. From the plume of plasma which contains rapid growth (formation initial stage) of clusters in the laser of plasma plume which that are nuclei for additional slow growth (formation of the intermediate stage) owing to diffusion of particles in the neighborhood of the clusters. Additional coagulation and coalescence,

If the growing is not influenced by the surfactants, takes place (formation late stage) conducting to the probable the agglomerations and precipitations. If the growth of particles from the phase of gaseous was spatially limited, this increases the probability for the surrounding particles diffusion to the neighborhood of embryologic particles, which lead to the formation of larger nanoparticles at the final stage of the growth. In other words, the length of diffusion for gaseous particles (Pb, O, Cu and atoms and ions) to the embryologic particle was smaller. It is expected that larger nano particles were created in deeper craters owing to the higher density of gaseous material ablated in spatially limited volume included in nanoparticles growth (higher possibility for growth of larger nanoparticles).

The elemental of composition for the nanoparticles was performed by energy dispersive X-ray spectroscopy (EDS). It was well-known which that ablation of the laser in such range of high pulse energy permit for ablation stoichiometric, the stoichiometry for bulk was mirrored into stoichiometry for ablated of plasma for plume (more nanoparticle growing takes place). It can be noted from the EDX spectrum in fig.7 , signals for lead, copper, silver, and oxygen appear with different percentages which listed in Table **shown** in the inset of Fig.7. It shows that there is an elevating of the percentage of oxygen in the prepared samples of deposited films. This might occur for the reason that more oxidization of (Pb, Cu, and Ag) as the plasma ion containing excitation energy within laser energy. Another reason can be catching of more atoms oxygen interior increasing of the grain boundary. In another word, there are

assigning to chemisorbed of oxygen ions, this matching with the results of the study.

Worthwhile, Fig.8 shows the micrographs of TEM images of the doped suspensions nanocolloidal of PbONPs, doping with fixed Cu and Ag concentrations (x=85%) obtained by PLAL in DI water. Histogram particle size distribution as shown in fig.9 and 10 for Cu and Ag dopping respectively, observed from these images that the average particles size for Ag NPs is around 12.6339nm, and 12.6339nm for Cu NPs as listed in table 3 that possess nanoparticle size. Spherical and small of non-uniform shapes of nanoparticles, a homogeneous structure without agglomeration which refers to ultrasonic process before the analysis. Thermal evaporation is the ablation mechanism related to pulsed laser ablation of the prepared target in liquids using a nanosecond pulsed laser. During PLAL pulse laser ablated in medium liquid, the laser beam wavelength and liquid medium influence the kinetics of nucleation and growth of nanoparticles leading to the formation of nanoparticles with different morphology, size, and structure. For a given target material and laser parameters, the particle was generated depends on the index refractive of the liquid surrounding at given laser wavelength. Lesser reflectivity for laser light at interface solid-liquid favoritisms ablation higher rate, through absorption of laser light by the liquid, diminishes ablation rate. Also, the growth procedures might be influenced by the liquid medium such as physical properties and at that point nanoparticles with dissimilar morphologies, size, and structure can result. It is stated that greatly polar molecules lean towards to form layers of an electrical double on the surface nanoparticles, stopping their growth, aggregation and then precipitation. Ablation time and can affect the productivity of nanoparticles and the continuous ablation of nanoparticles in the colloids can end with laser fragmentation to finer nanoparticles or melting of the nanoparticles to bigger ones depending on the energy and ablation wavelength [2-4]. In general, fabrication of nanoparticles depends on laser parameters, target material, and the nature of the liquid.

Polarity, viscosity, and the refractive index of the liquid at the ablation laser wavelength are important in determining the final size and size distribution. The decrease in size at higher ablation time can be due to the effect of continuous irradiation of particles in the colloidal solution at high laser energy fluence. But there was an increase in average size with increase in fluence for all the three liquid media. Increase in energy fluence could result in an increase in the average size of nanoparticles as reported in many cases [1-3, 8].

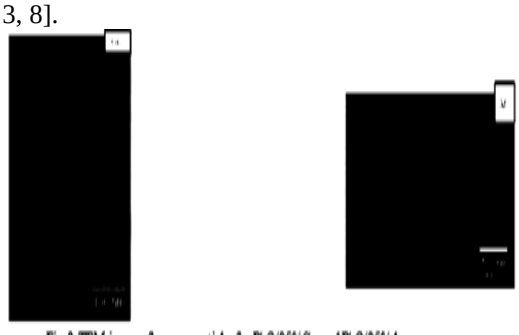

Fig.8 TEM images for nanoparticles for PbO/85%Cu and PbO/85%Ag.

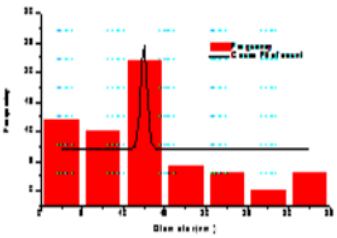

Fig.9 Histogram particle size distribution of 85%Cu

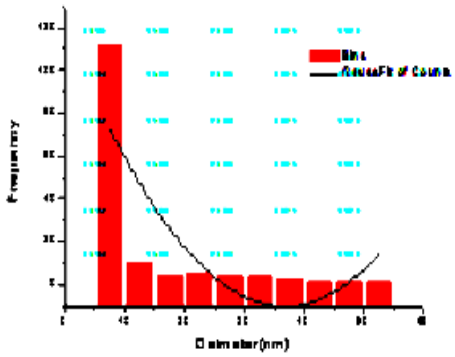

Fig.10 Histogram particle size distribution of 85%Ag

4. CONCLUSION

In summary, $PbO_{1-x}Cu_x$ and $PbO1_{-x}Ag_x$ nanoparticles NPS were successfully prepared by a pulsed laser ablation (PLAL) in deionized water. XRD analysis reveals that copper and silver ions are successfully introduced in Pb ions. XRD confirms lattice constants 'a' and '*c*' are decreased with increase in Cu, while these parameters increase in Ag doping. SEM and TEM images showed a well-defined spherical -like nanoparticles**.** TEM showed nanoparticles size of PbOCu 12.6339nm and for sample PbOAg 9.1624nm at a fixed percentage (85%).

5. REFERENCES

[1] Jacobsson, T. J. and Edvinsson, T., "Absorption and fluorescence spectroscopy of growing ZnO quantum dots: Size and band gap correlation and evidence of mobile trap states" *Inorg. Chem*, 50(19): 9578–9586 (2011).

[2] Chaudhuri,R. G. and Paria, S., "Core/shell nanoparticles: Classes, properties, synthesis mechanisms, characterization, and applications", *Chem. Rev*, 112(4) : 2373 (2012).

[3] Mahanti, M. and Basak, D., "Highly enhanced UV emission due to surface plasmon resonance in Ag–ZnO nanorods," *Chem.Phys. Lett*, 542(4): 110–116 (2012).

[4] Amendola, V. and Meneghetti, M., "hat control the composition and the structure of nanomaterials generated by laser ablation in liquid solution" *Phys. Chem. Chem. Phys*, 15(9): 3027–3046 (2013).

[5] Haider,A. J. , Shaker, S .S. and Asma H.M." A study of morphological, optical and gas sensing properties for pure and Ag-doped SnO2 prepared by pulsed laser

deposition (PLD) "*Energy Procedia*, 36:776–787(2013).

[6] Zeng, H. B., Du, X. W. Singh, S. C. et al., "Nanomaterials via laser ablation/irradiation in liquid: A review," *Adv. Funct. Mate*, 22(7): 1333–1353 (2012).

[7] Savchuk1, A.I., Stolyarchuk, I.D., Cieniek, B., "Optical Properties of Co-doped Zinc Oxide Nanoparticles, Prepared by Pulsed Laser Ablation in Liquids" *JOURNAL OF NANO- AND ELECTRONIC PHYSICS*", 7 (3),:03003(5pp) (2015).

[8] K. S. Khashan, M. S. Jabir, F A Abdulameer" Preparation and characterization of copper oxide nanoparticles decorated carbon nanoparticles using laser ablation in liquid" *IOP Conf. Series: Journal of Physics: Conf. Series*, 1003 (2018)

[9] Dunhua, C. Guangjun, Z. Jianyu, C. Qin, D. Yuchong, D.Yan, C. J. *Alloys Compd*., 489, 515(2010).

[10] Krstulovic, N., Salamon, K., Budimlija, O., "Parameters optimization for the synthesis of Al-doped ZnO nanoparticles by laser ablation in water", Applied *Surface Science* "440(3) :916–925(2018)

[11] García, G., Mendivil, M.I., Krishnan, B., Avellaneda, D., *Materials Chemistry and Physics*, 162(1): 561e570(2015).

[12] Kumar, L., Kumar, P., Narayan, A. and Ka,r M., "Rietveld analysis of XRD patterns of different sizes of nanocrystalline cobalt ferrite" *International Nano Letters* , 3:8(2013).